Neurochemistry International 131 (2019) 104541

Contents lists available at ScienceDirect

Neurochemistry International

journal homepage: www.elsevier.com/locate/neuint

Mitochondrial movement in Aralar/Slc25a12/AGC1 deficient cortical neurons

Guillermo Puertas-Frías[a], Araceli del Arco[b,c,d], Beatriz Pardo[a,c,d], Jorgina Satrústegui[a,c,d], Laura Contreras[a,c,d,*]

[a] Departamento de Biología Molecular, Centro de Biología Molecular Severo Ochoa UAM-CSIC, Universidad Autónoma de Madrid-Consejo Superior de Investigaciones Científicas, 28049, Madrid, Spain
[b] Facultad de Ciencias Ambientales y Bioquímica, Centro Regional de Investigaciones Biomédicas, Universidad de Castilla La Mancha, 45071, Toledo, Spain
[c] Instituto de Investigación Sanitaria Fundación Jiménez Díaz (IISFJD), 28049, Madrid, Spain
[d] Centro de Investigación Biomédica en Red de Enfermedades Raras (CIBERER), 28049, Madrid, Spain

ARTICLE INFO

Keywords:
Mitochondrial movement
Aralar/Slc25a12/AGC1
Glucose metabolism
Neuron

ABSTRACT

The elevated energy demands in the brain are fulfilled mainly by glucose catabolism. In highly polarized neurons, about 10–50% of mitochondria are transported along microtubules using mitochondrial-born ATP to locations with high energy requirements. In this report, we have investigated the impact of Aralar deficiency on mitochondrial transport in cultured cortical neurons. Aralar/slc25a12/AGC1 is the neuronal isoform of the aspartate-glutamate mitochondrial carrier, a component of the malate-aspartate shuttle (MAS) which plays an important role in redox balance, which is essential to maintain glycolytic pyruvate supply to neuronal mitochondria. Using live imaging microscopy we observed that the lack of Aralar does not affect the number of moving mitochondria nor the Ca^{2+}-induced stop, the only difference being a 10% increase in mitochondrial velocity in Aralar deficient neurons. Therefore, we evaluated the possible fuels used in each case by studying the relative contribution of oxidative phosphorylation and glycolysis to mitochondrial movement using specific inhibitors. We found that the ATP synthase inhibitor oligomycin caused a smaller inhibition of mitochondrial movement in Aralar-KO than control neurons, whereas the glycolysis inhibitor iodoacetate had similar effects in neurons from both genotypes. In line with these findings, the decrease in cytosolic ATP/ADP ratio caused by oligomycin was more pronounced in control than in Aralar-KO neurons, but no differences were observed with iodoacetate. Oligomycin effect was reverted by aralar re-expression in knock out cultures. As mitochondrial movement is not reduced in Aralar-KO neurons, these results suggest that these neurons may use an additional pathway for mitochondria movement and ATP/ADP ratio maintenance.

1. Introduction

Brain energy demand accounts for about 25% of body's resting glucose consumption, even if it represents only 2% of body weight (Belanger et al., 2011). Most of this energy fuels firing of action potentials and synaptic transmission, and it is provided mainly by glycolysis followed by pyruvate oxidation in mitochondria (Zsurka and Kunz, 2015). This represents a problem for the neurons, which are highly polarized cells with compartmentalized domains of high energetic demand over long distances, like Ranvier nodes and synaptic terminals. Because diffusion ratios of ADP and ATP are not high enough to comply with the high demand (de Graaf et al., 2000; Wallimann et al., 1992), the phosphocreatine/creatine kinase shuttle acts as a spatio-temporal buffer that provides energy to spots devoid of mitochondria (Fukumitsu et al., 2015). Alternatively, mitochondria may move to locations far from the cell body to provide ATP locally.

Most mitochondria remain stationary at areas with high energy demanding tasks, such as ion pumping or protein synthesis. However, 10–50% mitochondria are connected via adaptors like Miro1 to motor proteins of the kinesin or dynein families and are transported anterogradely (outside soma) or retrogradely (towards soma). How mitochondria are sorted between anterograde, retrograde or static pools is

Abbreviations: AGC, aspartate-glutamate carrier; DIV, days-in-vitro; GFP, green fluorescent protein; Glu, Glutamate; HBSS, HEPES buffered salt solution; IAA, iodoacetate; KO, knock out; MAS, malate aspartate shuttle; Olig, Oligomycin; OXPHOS, oxidative phosphorylation; WT, control or wild type

* Corresponding author. Departamento de Biología Molecular, Centro de Biología Molecular Severo Ochoa, CSIC-UAM, Universidad Autónoma de Madrid, C/ Nicolás Cabrera, 1, 28049, Madrid, Spain.
E-mail address: lcontreras@cbm.csic.es (L. Contreras).

https://doi.org/10.1016/j.neuint.2019.104541
Received 31 January 2019; Received in revised form 25 July 2019; Accepted 28 August 2019
Available online 28 August 2019
0197-0186/

still unresolved (Barnhart, 2016; Misgeld and Schwarz, 2017). Mitochondrial movement is carefully regulated, and regulation mechanisms often involve Ca^{2+} and energetic state (Lovas and Wang, 2013). In any event, alterations in mitochondrial trafficking (and dynamics) are often associated with neurodegenerative processes (Court and Coleman, 2012; Schon and Przedborski, 2011).

Studies in cultured neurons suggest that cytosolic Ca^{2+} rise results in a slowdown of mitochondrial movement. Ca^{2+} can be sensed by Miro1 (Macaskill et al., 2009; Saotome et al., 2008; Wang and Schwarz, 2009), a rho-GTPase inserted in the outer mitochondrial membrane, with EF-hands Ca^{2+} binding motifs facing the cytosol (Fransson et al., 2006; Niescier et al., 2013). However, cells without Miro1 maintained the Ca^{2+} regulation of mitochondrial movement (Nguyen et al., 2014), suggesting that other proteins, as Miro2, or mechanisms, like Ca^{2+} uptake into matrix (Chang et al., 2011), can also be involved.

Mitochondrial transport depends on an effective ATP production. Thus mitochondrial poisons such as uncouplers or inhibitors effectively reduce mitochondrial transport (Rintoul et al., 2003; Zala et al., 2013). This suggests that mitochondria are able to fuel their own transport unlike vesicle transport which relies on ATP produced in glycolysis (Zala et al., 2013). In an energized situation, cytosolic ATP levels support activity of motor proteins, but when the cytosolic ATP/ADP ratio decreases as result of high ATP demand, mitochondrial transport stops locally to increase ATP production and restore the ratio (Mironov, 2007).

Aralar/slc25a12/AGC1 is the neuronal isoform of the mitochondrial aspartate-glutamate carrier (AGC), whose activity is regulated by extramitochondrial Ca^{2+}(del Arco and Satrustegui, 1998; Satrustegui et al., 2007). AGC plays an important role in cell metabolism as component of the malate-aspartate shuttle (MAS) necessary to transfer redox equivalents from glycolysis to the mitochondrial matrix (Satrustegui et al., 2007). MAS activity serves a dual purpose: keeping the cytosolic redox balance for continuous glycolysis and pyruvate production, which in turn allows pyruvate supply for mitochondrial respiration, acting as a gas pedal regulated by Ca^{2+} (Llorente-Folch et al., 2013). This takes place by means of Ca^{2+}−activation of MAS via the EF-hand motifs present in AGC1 (Contreras et al., 2007; Marmol et al., 2008).

Aralar-KO mice lack MAS activity and have reduced mitochondrial O_2 consumption with glutamate/malate but normal respiration with substrates independent of MAS activity (Jalil et al., 2005). Accordingly, cultured cortical neurons lacking Aralar have a decrease of about 30–35% in glucose-fueled respiration under resting conditions and fail to enhance oxidative-phosphorylation (OXPHOS) in response to Ca^{2+} signals (Llorente-Folch et al., 2013).

In the present study, we have investigated the effect of Aralar deficiency on mitochondrial movement in cortical neurons under basal conditions and in response to glutamate-induced $[Ca^{2+}]_i$ transients. Having found that neither mitochondrial movement nor Ca^{2+}-dependent halt are disturbed by the lack of Aralar, despite the decreased glucose oxidative capacity of Aralar-KO neurons, we evaluated the contribution of glucose respiration and glycolysis to mitochondrial movement. We found a similar dependence on glycolysis albeit reduced dependence on respiration-born ATP for mitochondrial movement in Aralar-KO cortical neurons, when compared with control ones. Our results suggest that additional pathways different from OXPHOS or glycolysis but perhaps requiring the use of glucose derivatives, could be involved in fueling mitochondrial movement in the absence of Aralar.

2. Materials and methods

2.1. Animals

SVJ129-C57BL/6 mice carrying a disruption of the *aralar/slc25a12/agc1* gene (Jalil et al., 2005) were originally obtained from Lexicon Pharmaceuticals Inc. (The Woodlands, TX, USA) and have been maintained at the animal facility of the Center of Molecular Biology 'Severo Ochoa' ever since. Mice were housed in a humidity- and temperature-wild controlled room on a 12-h light/dark cycle, receiving water and food ad libitum. Genotype was determined by PCR using genomic DNA obtained from tail or embryonic tissue samples (Nucleospin tissue kit; Macherey-Nagel, Deuren, Germany) as described previously (Jalil et al., 2005). All animal procedures were approved by the corresponding institutional ethical Committee at the Center of Molecular Biology 'Severo Ochoa' and Autónoma University (CEEA-CBMSO-23/159) and were performed in accordance with Spanish regulations (BOE 67/8509–12, 1988) and European regulations (EU directive 86/609, EU decree 2001–486).

2.2. Neuronal culture

Cortical neuronal cultures were prepared from E15–E16 mouse embryos as described earlier by enzymatic and mechanical disgregation (Pardo et al., 2006; Ramos et al., 2003). Embryos were obtained from crosses between Aralar/slc25a12/AGC1 heterozygote mice and processed individually. Cells were plated in poly-L-lysine (50 μg/ml) and laminin (1 μg/ml) treated glass coverslips (Menzel Glässer, Braunschweig, Germany) or 4-well chamber slides (Lab-Tek, Thermo Fisher Scientific, Rochester, USA) at a density of $10^5/cm^2$ and maintained in Neurobasal medium supplemented with B27 (2%), glutamax (1%) (all from GIBCO Invitrogen, Carlsbad, CA, USA), penicillin (100 μg/ml) and streptomycin (100 U/ml) in a 5% CO_2 - 37 °C incubator. One-third of the medium was replaced every two-three days. Neurons represented > 80% of the total cell population (Pardo et al., 2006).

2.3. Mitochondrial movement

Neurons were incubated with Mitotracker Green (200 nM, 15 min) before transfer to pre-warmed HEPES Buffer salt solution (HBSS in mM: 137 NaCl, 5.4 KCl, 4.2 $NaHCO_3$, 2 $MgCl_2$, 0.8 KH_2PO_4, 10 HEPES, 2 $CaCl_2$, 5 glucose, pH 7.4) to visualize the complete mitochondrial network. Alternatively, neurons were transfected at 7–8 days in vitro (DIV) by the phosphate calcium protocol (Jiang and Chen, 2006) with plasmids coding for the green fluorescent protein (GFP) targeted to mitochondria (mitoGFP (Willers et al., 2012)) or co-transfected with vectors coding for mouse-Aralar (pcDNA3.1-Aralar, purchased from GenScript, USA) or the corresponding empty vector (pcDNA3.1, Invitrogene). On DIV 9–10, transfected cells were changed to pre-warmed HBSS and imaged at 37 °C on an Axiovert 200M inverted microscope equipped with a 40 × /1.3 Plan-Neofluor objective. The transfection method yields low efficiency (1–2% (Rintoul et al., 2003)), and allows to examine individual processes with clear association with a cell body to determine the direction of mitochondrial movement Retrograde movement was defined as mitochondria moving towards the soma and anterograde movement as moving away from the soma. No attempt was made to distinguish between axons and dendrites. Cells with fluorescent aggregates or excessive mitochondrial accumulation in the soma were not recorded. Cultures were excited for 100 ms at 472–27 (GFP) and emitted fluorescence was collected at 520/35 every 5 s using a filter wheel (Lambda 10–2, Sutter Instruments, all filters purchased from Chroma) and recorded by a Hamamatsu C9100-02 camera. Basal movement was recorded for 5 min before bolus addition of glutamate (Glu, 5 μM), oligomycin (Olig, 6 μM) or iodoacetate (IAA, 0.5 mM) from 10x stocks in HBSS; and recording continued for another 5 min. Experiments were then processed and analyzed using ImageJ software (NIH, Bethesda; http://rsb.info.nih.gov/ij/ (Abramoff et al., 2004)). All recordings were aligned using the "Align Slices" plugin and backgrounds were subtracted by default. Kymographs were obtained and analyzed using the plugins from J. Rietdorf (FMI Basel) and A. Seitz (EMBL, Heidelberg) (De Vos and Sheetz, 2007). Only mitochondria moving at > 0.01 μm/s were considered motile.

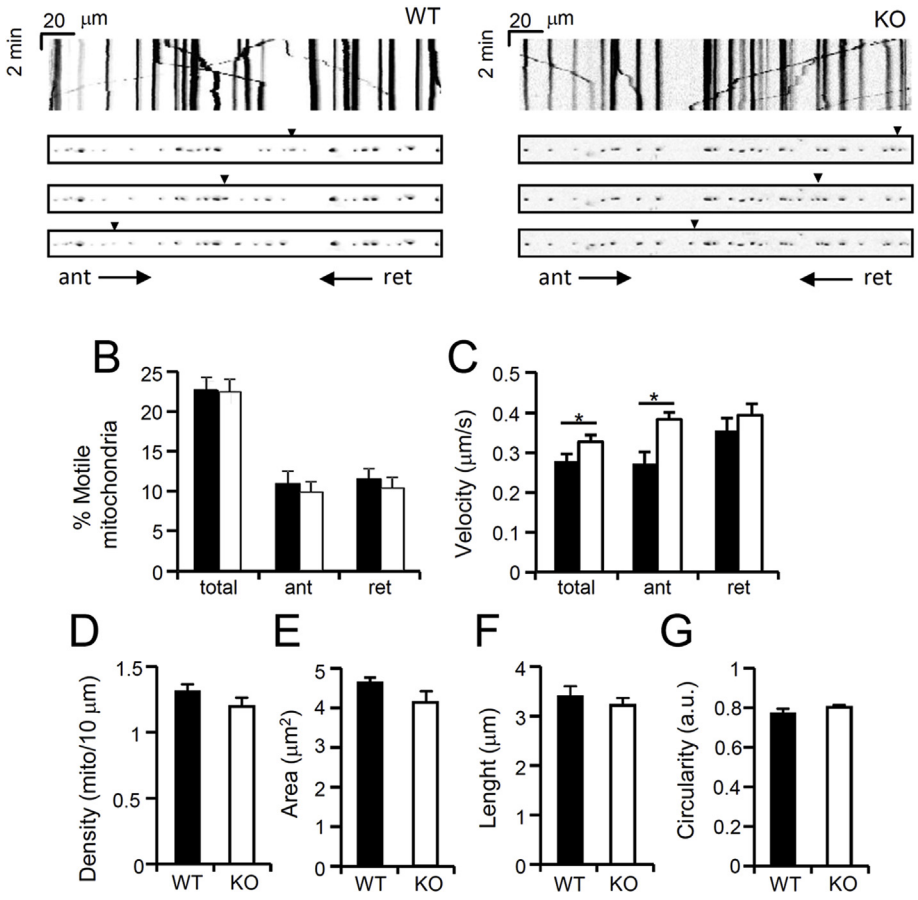

Fig. 1. Mitochondrial morphology and motility in control and Aralar-KO neuronal cortical cultures. Mitochondria movement and morphological parameters were determined in DIV 9–10 cortical neurons transiently transfected with mitoGFP to visualize mitochondrial structures. **A.** Representative kymographs of mitochondrial movement in a single neurite from control (WT) and Aralar-knock out (KO) cortical neurons. Vertical lines denote immobile mitochondria whereas lines with a positive slope are moving towards end feet (anterograde) and with a negative slope towards the soma (retrograde) Scale bars, 20 µm (abscissa axis) and 2 min (ordinate axis). **B.** Percentage of motile mitochondria as measured in kymographs (total) in the anterograde (ant) or retrograde (ret) direction. **C.** Average velocity (µm/s) of total mitochondria or mitochondria moving in the anterograde (ant) or retrograde (ret) direction. Data are average ± SEM of 18 independent cultures performed at least in duplicate and in parallel for each genotype (> 800 individual mitochondria). Statistical significance was evaluated using one-way ANOVA followed by Bonferroni's test, *$p < 0.05$. **D** Mitochondrial density, number of mitochondria present per 10 µm, n 13 independent platings. **E-G** The individual mitochondrial area, major axis length and circularity index were determined from 13 independent platings in parallel.

2.4. Mitochondrial morphology

Initial images from time-lapse recordings were analyzed with ImageJ to determine area, length and circularity of GFP expressing mitochondria (ImageJ "Analyze particles" plugin).

2.5. Measurement of ATP/ADP ratio

Single-cell measurements of cytosolic ATP/ADP ratio were obtained in neurons transfected using calcium phosphate protocol (DIV 7–8) with the plasmid coding for cytosolic ratiometric Perceval-HR (Tantama et al., 2013) or co-transfected with pcDNA3.1-Aralar, or the empty vector and used 36–48 h later. Experiments were performed in HBSS at 37 °C on an Axiovert 200M inverted microscope equipped with a 40 × /1.3 Plan-Neofluor objective. For Perceval-HR imaging, cells were excited every 5 s for 100–200 ms alternatively at 426–44 (Venus) and 472–27 (GFP); emitted fluorescence was collected at 520/35 (GFP). For basal detection of ATP/ADP, 20 images were acquired before bolus addition of oligomycin (6 µM), iodoacetate (0.5 mM) or both. Perceval-HR emission ratio was GFP/Venus reflecting cytosolic ATP/ADP ratio. Single-cell fluorescence recordings were analyzed using ImageJ and Excel software.

2.6. Measurement of cytosolic pH

Neurons were loaded with the fluorescent probe 2′, 7′-bis (2-carboxyethyl)-5 (6)-carboxy-fluorescein (BCECF; Invitrogen) in HBSS containing 0.25 µM BCECF-AM and 0.025% pluronic F.127 (Invitrogen) for 20 min at 37 °C. Excess probe was washed in HBSS for 20 min before use. Then, coverslips were mounted on the microscope stage equipped with a 40 × objective as described previously (Llorente-Folch et al., 2016) and BCECF fluorescence was imaged ratiometrically by using alternate excitation at 450 and 490 nm, and a 530 nm emission filter with a Neofluar 40 × /0.75 objective in an Axiovert 75M microscope (Zeiss). Additions were made as a bolus. For single-cell analysis of cytosolic pH, the ratio of fluorescence intensity at 450 nm (F_{450}) and 490 nm (F_{490}), (F_{450}/F_{490}), was obtained. Image acquisition was performed with the Aquacosmos 2.5 software (Hamamatsu), and data analysis was done with Image J and Excel software.

2.7. Cytosolic Ca^{2+} determination

Neurons growing on poly-L-lysine-coated coverslips were loaded with 5 µM Fura-2AM and 50 µM pluronic acid F.127 (Invitrogen) for 30 min at 37 °C in Ca^{2+}-free HBSS and washed for 30 min in HBSS with 2 mM Ca^{2+}. Experiments were done in HBSS the presence of 2 mM Ca^{2+}. Then coverslips were mounted on the microscope stage equipped with a 40× objective as described previously (Llorente-Folch et al., 2016) and Fura-2 fluorescence was imaged ratiometrically using alternate excitation at 340 and 380 nm, and a 510 nm emission filter with a Neofluar40x/0.75 objective in an Axiovert 75M microscope (Zeiss). The basal ratio was recorded before bolus addition of glutamate. For single-cell analysis of $[Ca^{2+}]i$ the ratio of fluorescence intensity at 340 nm (F_{340}) and 380 nm (F_{380}) (F_{340}/F_{380}) was obtained. Image acquisition was performed with the Aquacosmos 2.5 software (Hamamatsu) and data analysis was done with Aquacosmos 2.5 and Excel softwares.

2.8. Western blot analyses

DIV 9 cultured neurons were scrapped in RIPA buffer (TrisHCl 50 mM, NaCl 150 mM, Na^+-dodecyl sulphate 0.1%, Na^+-Deoxycholate 0.5%, TritonX-100 1%, 2 mM EDTA pH 7.8) to obtain total protein lysates. Sample proteins were separated by SDS-PAGE (10%)

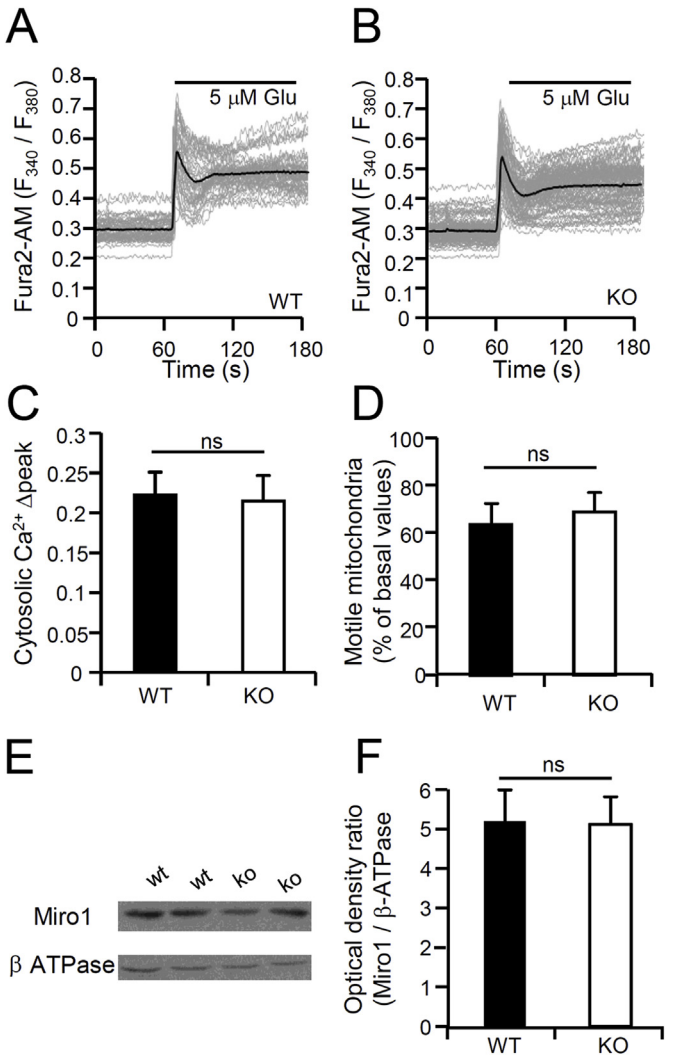

Fig. 2. Ca^{2+}-dependent inhibition of mitochondrial movement is not altered in Aralar-deficient neurons. A-C. Cytosolic Ca^{2+} responses to 5 μM glutamate stimulation in Fura-2 AM-loaded neurons, Representative experiments from control(**A**) and Aralar-KO (**B**) neurons show individual cell recordings (gray, 30–40 cells per assay) and average (black traces) are shown. **C.** Determination of glutamate induced Ca^{2+} peak in the cytosol between both genotypes. Data represent the average ± SEM of Ca^{2+} response from three independent cultures performed at least in triplicate per genotype. **D.** Percentage of motile mitochondria after 5 μM glutamate addition relative to basal movement (before glutamate addition). Data are average ± SEM of 4 independent neuronal cultures performed in triplicate (> 170 mitochondria per genotype). No statistical significant (ns) differences were observed (two-way ANOVA). **E.** Western blot analysis of whole brain mitochondria from 15-day old control (WT) and Aralar-KO (KO) mice per lane to detect Miro1. β-ATPase levels were used as loading control. **F.** Densitometric analysis of Miro1 protein levels shows no differences between genotypes. Data are the average ± SEM (n = 7 independent preparations) of Miro1 optical density (OD) normalized respect to their corresponding β − ATPase loading control.

electrophoresis, transferred onto NitroCellulose membranes and dyed with Ponceau Red, to assess for protein load. The membranes were blocked (5% Skim Milk, Nestlé) and probed with antibodies against Miro1/RhoT1 (Santa Cruz, sc-398520) and β-ATPase (Cuezva et al., 2002). After extensive washing, membranes were incubated with appropriate secondary antibodies conjugated with horseradish peroxidase and the signal was detected by chemiluminescence (ECL, PerkinElmer), as described earlier (del Arco et al., 2002). Analysis of resulting bands was performed with ImageJ software.

2.9. Immunocytochemistry

Transfected cells were fixed (4% Paraformaldehyde in PBS, 15 min), blocked (10% horse serum, 0,1% Triton-X100, 1 h) and incubated with polyclonal antibody raised against Aralar (1/250; del Arco and Satrustegui, 1998). After washing antibody excess, Alexa 555 (1/500, ThermoFisher) was used as secondary antibody. To visualize nuclei, DAPI (1 μg/ml; Merck) was used. No treatment to quench cell autofluorescence was used in order not to eliminate fluorescence of transfected mitoGFP or Perceval-HR, for which no antibodies were used. Images were obtained at Axiovert 200M inverted microscope equipped with a 40 × /1.3 Plan-Neofluor objective with appropriate filters.

2.10. Statistical analysis

The results are expressed as the mean ± standard error of the mean (SEM) of n independent cultures or preparations performed. All experiments were performed in parallel for each genotype. For basal (i.e. resting conditions before addition of compounds), all experiments were pooled. To determine the level of inhibition attained by the different compounds, each experiment was compared with its own basal activity. Statistical analysis indicated in Figure legends was performed with GraphPad Prism 7.00 or Origin 7.

3. Results & discussion

3.1. In cortical neurons, the percentage of motile mitochondria is unchanged in aralar deficiency, but mitochondria move faster

Mitochondrial movement is key to neuronal health as mitochondria fulfill roles in Ca^{2+} buffering (Macaskill et al., 2009), local dendritic and axonal protein synthesis (Cioni et al., 2019; Rangaraju et al., 2019), synaptic transmission (Lee and Peng, 2008; Li et al., 2004; Sun et al., 2013), and neurite branching and development (Lopez-Domenech et al., 2016; Smith and Gallo, 2018). Mutations in Aralar cause Global Cerebral Hypomyelination (OMIM # 612949) (Falk et al., 2014; Wibom et al., 2009) a rare disease whose features match well with the phenotype previously described in the Aralar-KO mice (Jalil et al., 2005).

As Aralar-KO neurons have a fall in basal and coupled respiration of 30–35% (Llorente-Folch et al., 2013), we hypothesized there would be also a decrease in mitochondrial movement, which is fueled mainly by oxidative phosphorylation derived ATP. The dependence from OXPHOS was derived from the impairment of mitochondrial motility when ATP-synthesis or mitochondrial respiration are inhibited (Borland et al., 2008; Rintoul et al., 2003; Rumora et al., 2017; Sterky et al., 2011; Zala et al., 2013). To test this hypothesis, we studied mitochondrial movement in control and Aralar-KO cortical neurons transiently transfected with the green fluorescent protein tagged to mitochondria (MitoGFP) (Fig. 1A).

Cortical neurons labeled with MitoGFP exhibited the complex behavior reported previously for mitochondrial movement, with mitochondria moving from and towards the soma. The fraction of motile mitochondria (22.47 ± 1.53%, Fig. 1B) and overall average velocity (0.28 ± 0.01 μm/s, Fig. 1C) observed in control cultures fall within the range of data previously reported (Misgeld and Schwarz, 2017). In addition, the fraction of mitochondria moving in each direction was also roughly the same (Fig. 1B). Aralar-KO neurons showed a similar percentage of motile mitochondria (22.25 ± 1.59%, Fig. 1B) but surprisingly, we found that mitochondria moved faster than control ones (0.32 ± 0.02 μm/s, $p < 0.05$, Fig. 1C), especially in the anterograde sense (Fig. 1C). Similar results were obtained when mitochondria were labeled with Mitotracker-Green (16.70 ± 1.77% and 15.87 ± 3.19% of motile mitochondria in control and Aralar-KO respectively, $p = 0.78$); with Aralar-KO moving slightly faster than control ones, (0.27 ± 0.01 versus 0.25 ± 0.01 μm/s respectively, $p < 0.05$). The similar percentage of motile mitochondria is consistent with the

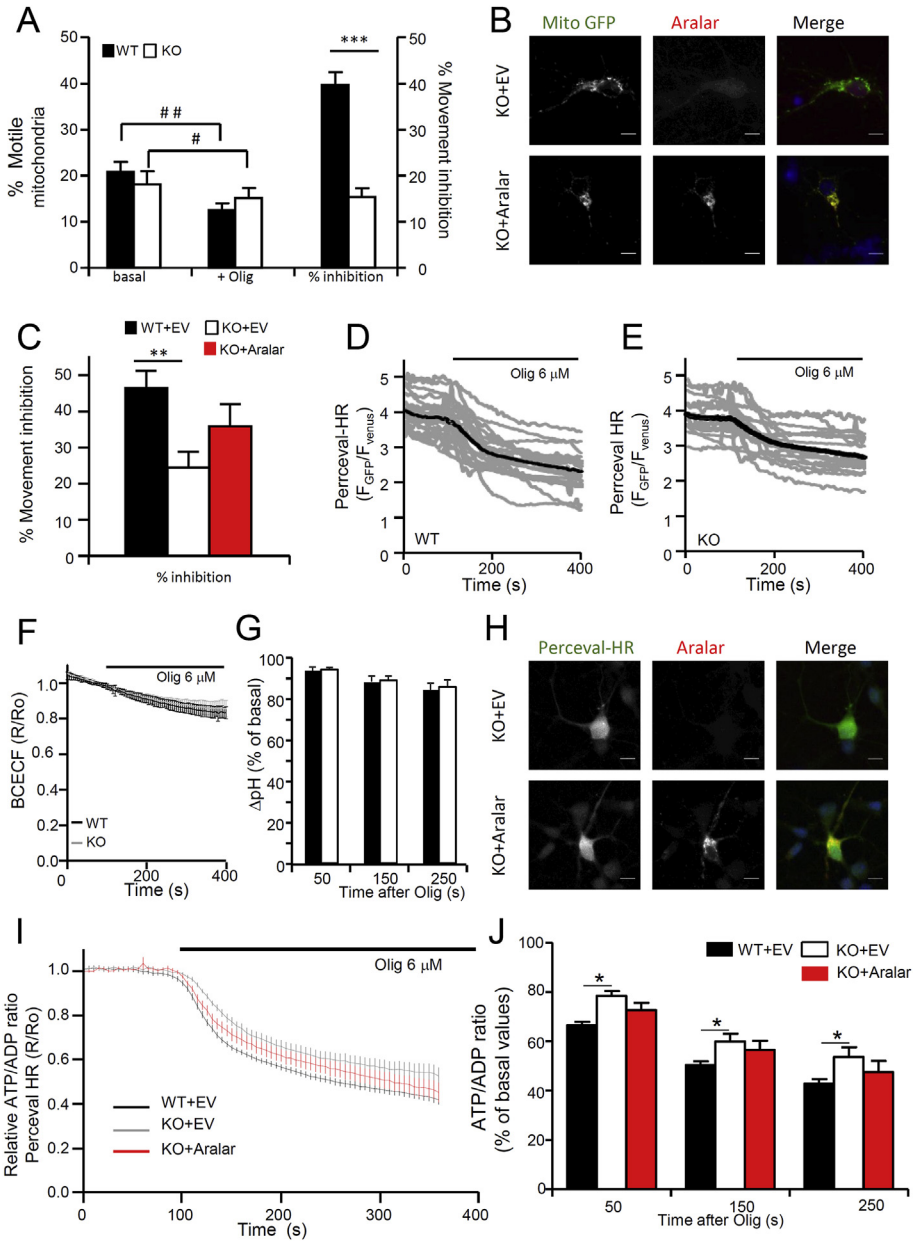

Fig. 3. Reduced dependence on mitochondrial ATP in Aralar-KO cortical neurons. A. Effect of Oligomycin addition on mitochondrial movement in control (WT) and Aralar-KO (KO) neurons. Motile mitochondria in basal condition and after oligomycin (6 µM) addition (left axis) and percentage of inhibition of movement (right axis). Data are mean ± SEM of 5 independent cultures. **B.** Immunocytochemistry of cultured neurons co-transfected with mitoGFP (green) and either empty vector (EV) pcDNA3 (KO + EV) or pcDNA3-Aralar plasmid (KO + Aralar) (red). Left panel shows the merge with nuclei in blue stained with DAPI. Scale bar is10 µm. **C.** Percentage of inhibition after oligomycin addition in WT and KO neurons transfected with the empty vector (WT + EV, KO + EV) and Aralar-Transfected KO (KO + Aralar) neurons. Data are mean ± SEM of 5 independent platings. Two-way ANOVA followed by Bonferroni's test **p < 0.05. **D,E.** Oligomycin-induced changes in ATP/ADP ratio in control (**D**) and Aralar-KO (**E**) neurons transfected with the ratiometric probe Perceval-HR. Perceval-HR occupancy is shown as GFP/Venus fluorescence ratio and oligomycin addition is indicated. Average (black) and individual neurons (gray) are depicted. **F** Cytosolic pH variations measured with BCECF-AM upon oligomycin addition in WT (black) or KO (gray) neurons. **G.** Quantification of pH at indicated times after Oligomycin addition. Data correspond to mean F_{490}/F_{440} ratio (R/R_0) from 3 independent cultures performed in triplicate. No significant differences found (Repeated-Measures ANOVA). **I.** Immunocytochemistry of cultured neurons co-transfected with Perceval-HR (green) and either empty vector (KO + EV) or pcDNA3-Aralar plasmid (KO + Aralar) (red). Left panel shows the merge with nuclei in blue stained with DAPI. Scale bar is10 µm. **K.** Quantification of cytosolic ATP/ADP ratio in control (WT + EV), Aralar-KO (KO + EV) and Aralar-transfected KO (KO + Aralar) neurons at different time points after addition of oligomycin. Data are mean ± SEM from 4 independent platings. Data were analyzed Two-way ANOVA Repeated measures, followed by Bonferroni's test. (basal vs. oligo #p < 0.05, # #p < 0.005; WT vs KO, *p < 0.05; **p < 0.005; ***p < 0.0005).

equivalent density of mitochondria observed along the neurites (Fig. 1D), and with the lack of differences in mitochondrial morphology (Fig. 1E–G) that would compromise their movement (Kaasik et al., 2007; Trevisan et al., 2018).

Therefore, absence of Aralar does not cause an impairment of mitochondrial movement but rather a slight increase in anterograde velocity. Accordingly, in a recent study using a transgenic Aralar model showing a slight overexpression of Aralar in brain a decrease in mitochondrial run length and processivity was observed (Haziza et al., 2017), suggesting a possible role for Aralar in the regulation of mitochondrial movement.

3.2. Aralar deficient mitochondria are halted by calcium signal as in control neurons

Ca^{2+}-regulation of Aralar activity may participate in the regulation of mitochondrial movement by Ca^{2+} signals, by acting as secondary mitochondrial Ca^{2+} sensor to halt or slowdown mitochondria at high [Ca^{2+}] regions where energy is required. It is established that cytosolic calcium acting through Miro1 (Macaskill et al., 2009; Saotome et al., 2008; Wang and Schwarz, 2009) regulate mitochondrial movement. However, a role for Miro1 in Ca^{2+}-regulated mitochondrial trafficking has recently been challenged (Nguyen et al., 2014), suggesting that other mitochondrial Ca^{2+}-binding proteins could participate in the regulation. Indeed, Miro1 and Aralar have a similar affinity for cytosolic calcium (≈300 nM (Contreras et al., 2007; Saotome et al., 2008)), opening the possibility that Aralar may also contribute to mitochondrial stopping at high Ca^{2+} domains to fuel energy demands, and its absence would result in higher motility.

To address this hypothesis, we examined the motility of mitochondria in control and Aralar-deficient neurons in response to glutamate-induced calcium signals. In neurons, the absence of Aralar does not cause alterations in resting Ca^{2+} levels or in the response to glutamate (Llorente-Folch et al., 2013, 2016), Fig. 2A–C). As shown in Fig. 2A–C, non-excitotoxic glutamate concentrations (5 µM) (Llorente-Folch et al., 2016) which activate both ionotropic and metabotropic receptors trigger a similar Ca^{2+} transient in cortical neurons from both genotypes. In agreement with previous results (Chang et al., 2006; Rintoul

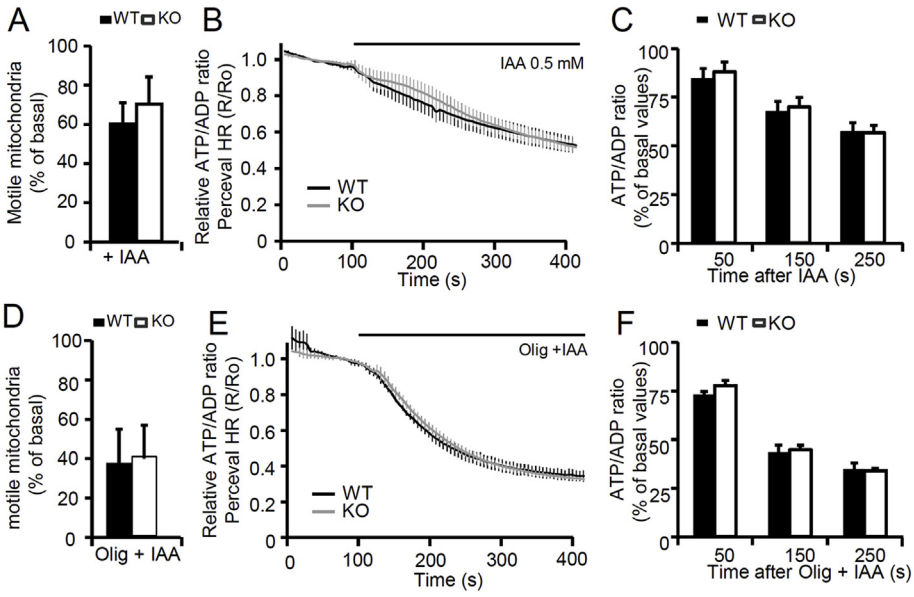

Fig. 4. Inhibition of glycolysis reduces mitochondrial movement in control and Aralar-KO neurons. A. Percentage of motile mitochondria in control (WT) and Aralar-KO (KO) neurons after the addition of 0.5 mM IAA normalized to basal conditions. Data are shown as average ± SEM from n = 6 independent cultures performed in parallel (> 130 mitochondria). **B.** ATP/ADP ratio in WT (black) and KO (gray) neurons changes after IAA addition in Perceval-HR transfected cutlures. **C.** Quantification of ATP/ADP at indicated times of IAA addition. Data are average of 8 independent platings. **D.** Percentage of motile mitochondria in control (WT) and Aralar-KO (KO) neurons after the addition of oligomycin + IAA normalized to basal conditions. Data are shown as mean ± SEM from n = 3 independent cultures performed in parallel. **E.** ATP/ADP ratio in WT (black) and KO (gray) neurons changes after IAA addition in Perceval-HR transfected cultures. **F.** Quantification of cytosolic ATP/ADP ratio in WT and KO neurons at different time points after addition of Oligomycin + IAA. Data are mean ± SEM of 3 independent platings. No statistical significance (ns) was found between genotypes (two-way ANOVA analysis).

et al., 2003; Wang and Schwarz, 2009), exposure to glutamate caused a decrease in mitochondrial movement. This decrease was similar in control and Aralar-KO neurons with a reduction of motile mitochondria to 63.05 ± 8.82% and 68.24 ± 7.47% of basal values respectively (Fig. 2D). In agreement, the levels of Miro1/RhoT1, the Ca^{2+} sensor of mitochondrial movement, were unchanged in Aralar-KO neurons (Fig. 2E and F). These results rule out an involvement of Aralar in mitochondrial halting in response to Ca^{2+} transient signals, and open the question of how mitochondrial movement is fueled in Aralar-KO neurons.

3.3. Mitochondrial movement in Aralar-KO neurons has a reduced dependence on OXPHOS-derived ATP

First, we tested the dependence on OXPHOS-derived ATP on mitochondrial motility in Aralar-KO neurons. We treated cortical neurons with 6 μM oligomycin, an inhibitor of mitochondrial ATP synthase and examined mitochondrial movement. Oligomycin caused a decrease in the fraction of motile mitochondria in control neurons (to 60.26 ± 3.11% of basal values, Fig. 3A) without significant changes in the directionality of movement or velocity (not shown). Vehicle addition had no effect on mitochondrial velocity or number of moving mitochondria (not shown). However, the effect of oligomycin addition was less pronounced in Aralar-KO (the fraction of moving mitochondria only decreased to 84.62 ± 2.14% of basal values, Fig. 3A). We next re-expressed Aralar by co-transfection with mitoGFP (Fig. 3B) and studied its effect 48 h later on oligomycin arrested movement. We observed that, Aralar re-expression in *knock-out* cultures increased the effect of oligomycin (65.44 ± 6.02% of motile mitochondria compared to basal values) (Fig. 3C). These results suggest that mitochondrial movement in Aralar-KO cortical neurons has a lower dependence on OXPHOS as energy supplier than control neurons, at least when glucose is the substrate available.

The ATP/ADP ratio has been proposed to play a role in regulating mitochondrial transport velocity (Mironov, 2007). Therefore, we next addressed whether cytosolic ATP levels were differently affected by ATP synthase inhibition in Aralar-KO and control neurons using the ratiometric ATP/ADP biosensor Perceval-HR (Tantama et al., 2013), No differences in basal Perceval-HR fluorescence ratios were observed (3.73 ± 0.13 in control versus 3.70 ± 0.10 in Aralar-KO neurons), as reported previously (Llorente-Folch et al., 2016). (Fig. 3D and E), but oligomycin induced a decrease in the ratio. As Perceval-HR fluorescence is pH-sensitive, we have first verified that differences in oligomycin-induced acidification were not responsible for the differential drop in the ATP/ADP ratio. Cytosolic pH recordings obtained in BCECF-AM loaded neurons indicate that the slight acidification induced by oligomycin was the same in KO and control neurons (Fig. 3F and G). Vehicle addition had no effect on the ATP/ADP ratio (not shown). However, the addition of oligomycin induced a significant drop in the ATP/ADP ratio more pronounced in control than Aralar-KO neurons (to 42.88 ± 0.03% and 55.6 ± 0.04% of initial values, respectively after 250 s compare traces in D, E). Furthermore, Aralar re-expression by co-transfection with Perceval-HR (Fig. 3H) resulted in a similar decrease in ATP/ADP ratio to control cultures at the different time points evaluated (Fig. 3J). The results are consistent with the effect on movement observed in Aralar-KO and control neurons upon oligomycin addition, and also with the absence of differences in the ATP/ADP ratio and number of motile mitochondria in basal conditions between genotypes. Although the recovery due to re-expression of Aralar in KO cultures was not complete, taken together, these data suggest a lesser dependence on OXPHOS as fuel for mitochondrial movement and ATP/ADP ratio maintenance in Aralar-KO neurons, suggesting that Aralar deficiency may be compensated by other energy pathways for the maintenance of ATP/ADP ratio. These sources may also be used for the purpose of fueling mitochondrial movement in Aralar-KO neurons.

3.4. Glycolysis inhibition decreases mitochondrial movement both in control and Aralar-KO neurons

Next, we evaluated a possible compensation by the ATP generated in the glycolysis. Although mitochondrial respiration provides most of the ATP used in the brain, glycolysis has been recognized as an alternative power-source for a number of cellular tasks. Indeed, glycolytic-born ATP is used to fuel fast transport of cargo vesicles (Zala et al., 2013), to sustain synaptic activity (Chavan et al., 2015; Jang et al., 2016; Rangaraju et al., 2014) and also to upload glutamate into synaptic vesicles (Ikemoto et al., 2003). Therefore, we tested whether glycolysis can provide ATP to sustain mitochondria movement in Aralar-KO neurons more efficiently than in control neurons.

To study the contribution of glycolytic-derived ATP to mitochondrial movement, we inhibited glycolysis at the level of the glyceraldehyde-3-phosphate dehydrogenase (GAPDH) with iodoacetate (IAA), a commonly used pharmacological inhibitor for this target (Diaz-Garcia et al., 2017). We found that in the presence of 0.5 mM IAA the

percentage of motile mitochondria is reduced equally in both genotypes (Fig. 4 A), as was the velocity of movement in (not shown). Similarly, IAA-dependent decrease of the ATP/ADP ratio, as evaluated using the ratiometric ATP/ADP biosensor Perceval-HR (Tantama et al., 2013), was identical in both genotypes (Fig. 4B and C).

Addition of both inhibitors together (IAA + Olig) decreased mitochondrial movement (Fig. 4 D), velocity (not shown) and ATP/ADP ratios (Fig. 4E and F) to a larger extent than the addition of each of these compounds separately, such a treatment is expected to block most of the ATP synthesis pathways and will also deprive neurons from substrates required to feed any alternative energy pathway, resulting in a complete energy rundown regardless of the genotype.

In sum, these results argue against a preferential use of glycolysis in Aralar-KO neurons and suggest that additional pathways different from OXPHOS or glycolysis but perhaps requiring the use of glucose derivatives, could be involved in fueling mitochondrial movement in the absence of Aralar.

4. Conclusions

Mitochondria in Aralar-KO neurons move to a similar extent, and even faster, than in control neurons, despite the fact that glucose respiration is reduced in absence of Aralar. This result was surprising as mitochondrial movement has been shown to depend highly on ATP of mitochondrial origin. In this report, we have demonstrated that Aralar-KO neurons are less dependent on ATP produced by mitochondrial respiration, when the substrate available is glucose, than control neurons, at least for the purpose of fueling movement of mitochondria and maintenance of basal ATP/ADP ratio, but they require nonetheless glycolysis to the same extent as control neurons.

Acknowledgements

The authors thank Barbara Sesé, Isabel Manso, Alba del Río-Lorenzo and the Optical and Confocal Microscopy unit of the CBMSO for their support. This work was supported by grants S2010/BMD-2402, and a grant from Fundación Ramón Areces to JS; SAF2014-56929R to JS and BP; SAF2017-82560-R to BP and AdA and an institutional grant from Fundación Ramón Areces to the Centro de Biología Molecular Severo Ochoa. LC has been the recipient of a Junta de Ampliación de Estudios-Consejo Superior de Investigaciones Científicas and CIBERER postdoctoral contracts. The authors declare no competing financial interests.

References

Abramoff, M.D., MagalHaes, P.J., Ram, S.J., 2004. Image processing with image. Biophot. Int. 11, 36–42.
Barnhart, E.L., 2016. Mechanics of mitochondrial motility in neurons. Curr. Opin. Cell Biol. 38, 90–99.
Belanger, M., Allaman, I., Magistretti, P.J., 2011. Brain energy metabolism: focus on astrocyte-neuron metabolic cooperation. Cell Metabol. 14, 724–738.
Borland, M.K., Trimmer, P.A., Rubinstein, J.D., Keeney, P.M., Mohanakumar, K., Liu, L., Bennett Jr., J.P., 2008. Chronic, low-dose rotenone reproduces Lewy neurites found in early stages of Parkinson's disease, reduces mitochondrial movement and slowly kills differentiated SH-SY5Y neural cells. Mol. Neurodegener. 3, 21.
Cioni, J.M., Lin, J.Q., Holtermann, A.V., Koppers, M., Jakobs, M.A.H., Azizi, A., Turner-Bridger, B., Shigeoka, T., Franze, K., Harris, W.A., Holt, C.E., 2019. Late endosomes act as mRNA translation platforms and sustain mitochondria in axons. Cell 176, 56–72 e15.
Contreras, L., Gomez-Puertas, P., Iijima, M., Kobayashi, K., Saheki, T., Satrustegui, J., 2007. Ca2+ Activation kinetics of the two aspartate-glutamate mitochondrial carriers, aralar and citrin: role in the heart malate-aspartate NADH shuttle. J. Biol. Chem. 282, 7098–7106.
Court, F.A., Coleman, M.P., 2012. Mitochondria as a central sensor for axonal degenerative stimuli. Trends Neurosci. 35, 364–372.
Cuezva, J.M., Krajewska, M., de Heredia, M.L., Krajewski, S., Santamaria, G., Kim, H., Zapata, J.M., Marusawa, H., Chamorro, M., Reed, J.C., 2002. The bioenergetic signature of cancer: a marker of tumor progression. Cancer Res. 62, 6674–6681.
Chang, D.T., Honick, A.S., Reynolds, I.J., 2006. Mitochondrial trafficking to synapses in cultured primary cortical neurons. J. Neurosci. 26, 7035–7045.
Chang, K.T., Niescier, R.F., Min, K.T., 2011. Mitochondrial matrix Ca2+ as an intrinsic signal regulating mitochondrial motility in axons. Proc. Natl. Acad. Sci. U. S. A. 108, 15456–15461.
Chavan, V., Willis, J., Walker, S.K., Clark, H.R., Liu, X., Fox, M.A., Srivastava, S., Mukherjee, K., 2015. Central presynaptic terminals are enriched in ATP but the majority lack mitochondria. PLoS One 10, e0125185.
de Graaf, R.A., van Kranenburg, A., Nicolay, K., 2000. In vivo (31)P-NMR diffusion spectroscopy of ATP and phosphocreatine in rat skeletal muscle. Biophys. J. 78, 1657–1664.
De Vos, K.J., Sheetz, M.P., 2007. Visualization and quantification of mitochondrial dynamics in living animal cells. Methods Cell Biol. 80, 627–682.
del Arco, A., Morcillo, J., Martinez-Morales, J.R., Galian, C., Martos, V., Bovolenta, P., Satrustegui, J., 2002. Expression of the aspartate/glutamate mitochondrial carriers aralar1 and citrin during development and in adult rat tissues. Eur. J. Biochem. 269, 3313–3320.
del Arco, A., Satrustegui, J., 1998. Molecular cloning of Aralar, a new member of the mitochondrial carrier superfamily that binds calcium and is present in human muscle and brain. J. Biol. Chem. 273, 23327–23334.
Diaz-Garcia, C.M., Mongeon, R., Lahmann, C., Koveal, D., Zucker, H., Yellen, G., 2017. Neuronal stimulation triggers neuronal glycolysis and not lactate uptake. Cell Metabol. 26, 361–374 e364.
Falk, M.J., Li, D., Gai, X., McCormick, E., Place, E., Lasorsa, F.M., Otieno, F.G., Hou, C., Kim, C.E., Abdel-Magid, N., Vazquez, L., Mentch, F.D., Chiavacci, R., Liang, J., Liu, X., Jiang, H., Giannuzzi, G., Marsh, E.D., Yiran, G., Tian, L., Palmieri, F., Hakonarson, H., 2014. AGC1 deficiency causes infantile epilepsy, abnormal myelination, and reduced N-acetylaspartate. JIMD Rep. 14, 77–85.
Fransson, S., Ruusala, A., Aspenstrom, P., 2006. The atypical Rho GTPases Miro-1 and Miro-2 have essential roles in mitochondrial trafficking. Biochem. Biophys. Res. Commun. 344, 500–510.
Fukumitsu, K., Fujishima, K., Yoshimura, A., Wu, Y.K., Heuser, J., Kengaku, M., 2015. Synergistic action of dendritic mitochondria and creatine kinase maintains ATP homeostasis and actin dynamics in growing neuronal dendrites. J. Neurosci. 35, 5707–5723.
Haziza, S., Mohan, N., Loe-Mie, Y., Lepagnol-Bestel, A.M., Massou, S., Adam, M.P., Le, X.L., Viard, J., Plancon, C., Daudin, R., Koebel, P., Dorard, E., Rose, C., Hsieh, F.J., Wu, C.C., Potier, B., Herault, Y., Sala, C., Corvin, A., Allinquant, B., Chang, H.C., Treussart, F., Simonneau, M., 2017. Fluorescent nanodiamond tracking reveals intraneuronal transport abnormalities induced by brain-disease-related genetic risk factors. Nat. Nanotechnol. 12, 322–328.
Ikemoto, A., Bole, D.G., Ueda, T., 2003. Glycolysis and glutamate accumulation into synaptic vesicles. Role of glyceraldehyde phosphate dehydrogenase and 3-phosphoglycerate kinase. J. Biol. Chem. 278, 5929–5940.
Jalil, M.A., Begum, L., Contreras, L., Pardo, B., Iijima, M., Li, M.X., Ramos, M., Marmol, P., Horiuchi, M., Shimotsu, K., Nakagawa, S., Okubo, A., Sameshima, M., Isashiki, Y., Del Arco, A., Kobayashi, K., Satrustegui, J., Saheki, T., 2005. Reduced N-acetylaspartate levels in mice lacking aralar, a brain- and muscle-type mitochondrial aspartate-glutamate carrier. J. Biol. Chem. 280, 31333–31339.
Jang, S., Nelson, J.C., Bend, E.G., Rodriguez-Laureano, L., Tueros, F.G., Cartagenova, L., Underwood, K., Jorgensen, E.M., Colon-Ramos, D.A., 2016. Glycolytic enzymes localize to synapses under energy stress to support synaptic function. Neuron 90, 278–291.
Jiang, M., Chen, G., 2006. High Ca2+-phosphate transfection efficiency in low-density neuronal cultures. Nat. Protoc. 1, 695–700.
Kaasik, A., Safiulina, D., Choubey, V., Kuum, M., Zharkovsky, A., Veksler, V., 2007. Mitochondrial swelling impairs the transport of organelles in cerebellar granule neurons. J. Biol. Chem. 282, 32821–32826.
Lee, C.W., Peng, H.B., 2008. The function of mitochondria in presynaptic development at the neuromuscular junction. Mol. Biol. Cell 19, 150–158.
Li, Z., Okamoto, K., Hayashi, Y., Sheng, M., 2004. The importance of dendritic mitochondria in the morphogenesis and plasticity of spines and synapses. Cell 119, 873–887.
Lopez-Domenech, G., Higgs, N.F., Vaccaro, V., Ros, H., Arancibia-Carcamo, I.L., MacAskill, A.F., Kittler, J.T., 2016. Loss of dendritic complexity precedes neurodegeneration in a mouse model with disrupted mitochondrial distribution in mature dendrites. Cell Rep. 17, 317–327.
Lovas, J.R., Wang, X., 2013. The meaning of mitochondrial movement to a neuron's life. Biochim. Biophys. Acta 1833, 184–194.
Llorente-Folch, I., Rueda, C.B., Amigo, I., del Arco, A., Saheki, T., Pardo, B., Satrustegui, J., 2013. Calcium-regulation of mitochondrial respiration maintains ATP homeostasis and requires ARALAR/AGC1-malate aspartate shuttle in intact cortical neurons. J. Neurosci. 33, 13957–13971 13971a.
Llorente-Folch, I., Rueda, C.B., Perez-Liebana, I., Satrustegui, J., Pardo, B., 2016. L-Lactate-Mediated neuroprotection against glutamate-induced excitotoxicity requires ARALAR/AGC1. J. Neurosci. 36, 4443–4456.
Macaskill, A.F., Rinholm, J.E., Twelvetrees, A.E., Arancibia-Carcamo, I.L., Muir, J., Fransson, A., Aspenstrom, P., Attwell, D., Kittler, J.T., 2009. Miro1 is a calcium sensor for glutamate receptor-dependent localization of mitochondria at synapses. Neuron 61, 541–555.
Marmol, P., Pardo, B., Wiederkehr, A., Del Arco, A., Wollheim, C.B., Satrustegui, J., 2008. Requirement for aralar and its Ca2+-binding sites in Ca2+-signal transduction in mitochondria from INS-1 clonal beta -cells. J. Biol. Chem. 284, 515–524.
Mironov, S.L., 2007. ADP regulates movements of mitochondria in neurons. Biophys. J. 92, 2944–2952.
Misgeld, T., Schwarz, T.L., 2017. Mitostasis in neurons: maintaining mitochondria in an extended cellular architecture. Neuron 96, 651–666.
Nguyen, T.T., Oh, S.S., Weaver, D., Lewandowska, A., Maxfield, D., Schuler, M.H., Smith,

N.K., Macfarlane, J., Saunders, G., Palmer, C.A., Debattisti, V., Koshiba, T., Pulst, S., Feldman, E.L., Hajnoczky, G., Shaw, J.M., 2014. Loss of Miro1-directed mitochondrial movement results in a novel murine model for neuron disease. Proc. Natl. Acad. Sci. U. S. A. 111, E3631–E3640.
Niescier, R.F., Chang, K.T., Min, K.T., 2013. Miro, MCU, and calcium: bridging our understanding of mitochondrial movement in axons. Front. Cell. Neurosci. 7, 148.
Pardo, B., Contreras, L., Serrano, A., Ramos, M., Kobayashi, K., Iijima, M., Saheki, T., Satrustegui, J., 2006. Essential role of aralar in the transduction of small Ca2+ signals to neuronal mitochondria. J. Biol. Chem. 281, 1039–1047.
Ramos, M., del Arco, A., Pardo, B., Martinez-Serrano, A., Martinez-Morales, J.R., Kobayashi, K., Yasuda, T., Bogonez, E., Bovolenta, P., Saheki, T., Satrustegui, J., 2003. Developmental changes in the Ca2+-regulated mitochondrial aspartate-glutamate carrier aralar1 in brain and prominent expression in the spinal cord. Brain Res. Dev. Brain Res. 143, 33–46.
Rangaraju, V., Calloway, N., Ryan, T.A., 2014. Activity-driven local ATP synthesis is required for synaptic function. Cell 156, 825–835.
Rangaraju, V., Lauterbach, M., Schuman, E.M., 2019. Spatially stable mitochondrial compartments fuel local translation during plasticity. Cell 176, 73–84 e15.
Rintoul, G.L., Filiano, A.J., Brocard, J.B., Kress, G.J., Reynolds, I.J., 2003. Glutamate decreases mitochondrial size and movement in primary forebrain neurons. J. Neurosci. 23, 7881–7888.
Rumora, A.E., Lentz, S.I., Hinder, L.M., Jackson, S.W., Valesano, A., Levinson, G.E., Feldman, E.L., 2017. Dyslipidemia impairs mitochondrial trafficking and function in sensory neurons. FASEB J. 32, 195–207.
Saotome, M., Safiulina, D., Szabadkai, G., Das, S., Fransson, A., Aspenstrom, P., Rizzuto, R., Hajnoczky, G., 2008. Bidirectional Ca2+-dependent control of mitochondrial dynamics by the Miro GTPase. Proc. Natl. Acad. Sci. U. S. A. 105, 20728–20733.
Satrustegui, J., Pardo, B., Del Arco, A., 2007. Mitochondrial transporters as novel targets for intracellular calcium signaling. Physiol. Rev. 87, 29–67.
Schon, E.A., Przedborski, S., 2011. Mitochondria: the next (neurode)generation. Neuron 70, 1033–1053.
Smith, G.M., Gallo, G., 2018. The role of mitochondria in axon development and regeneration. Dev. Neurobiol. 78, 221–237.
Sterky, F.H., Lee, S., Wibom, R., Olson, L., Larsson, N.G., 2011. Impaired mitochondrial transport and Parkin-independent degeneration of respiratory chain-deficient dopamine neurons in vivo. Proc. Natl. Acad. Sci. U. S. A. 108, 12937–12942.
Sun, T., Qiao, H., Pan, P.Y., Chen, Y., Sheng, Z.H., 2013. Motile axonal mitochondria contribute to the variability of presynaptic strength. Cell Rep. 4, 413–419.
Tantama, M., Martinez-Francois, J.R., Mongeon, R., Yellen, G., 2013. Imaging energy status in live cells with a fluorescent biosensor of the intracellular ATP-to-ADP ratio. Nat. Commun. 4, 2550.
Trevisan, T., Pendin, D., Montagna, A., Bova, S., Ghelli, A.M., Daga, A., 2018. Manipulation of mitochondria dynamics reveals separate roles for form and function in mitochondria distribution. Cell Rep. 23, 1742–1753.
Wallimann, T., Wyss, M., Brdiczka, D., Nicolay, K., Eppenberger, H.M., 1992. Intracellular compartmentation, structure and function of creatine kinase isoenzymes in tissues with high and fluctuating energy demands: the 'phosphocreatine circuit' for cellular energy homeostasis. Biochem. J. 281 (Pt 1), 21–40.
Wang, X., Schwarz, T.L., 2009. The mechanism of Ca2+ -dependent regulation of kinesin-mediated mitochondrial motility. Cell 136, 163–174.
Wibom, R., Lasorsa, F.M., Tohonen, V., Barbaro, M., Sterky, F.H., Kucinski, T., Naess, K., Jonsson, M., Pierri, C.L., Palmieri, F., Wedell, A., 2009. AGC1 deficiency associated with global cerebral hypomyelination. N. Engl. J. Med. 361, 489–495.
Willers, I.M., Martinez-Reyes, I., Martinez-Diez, M., Cuezva, J.M., 2012. miR-127-5p targets the 3'UTR of human beta-F1-ATPase mRNA and inhibits its translation. Biochim. Biophys. Acta 1817, 838–848.
Zala, D., Hinckelmann, M.V., Yu, H., Lyra da Cunha, M.M., Liot, G., Cordelieres, F.P., Marco, S., Saudou, F., 2013. Vesicular glycolysis provides on-board energy for fast axonal transport. Cell 152, 479–491.
Zsurka, G., Kunz, W.S., 2015. Mitochondrial dysfunction and seizures: the neuronal energy crisis. Lancet Neurol. 14, 956–966.